System Identification of Hydrostatic Transmission (HST) System Using Bond Graph Methodology

Sarnendu Paul, Arghya Mondal, Abhishek Guha, and Priyanshu Kumar Dubey

1 System Description

The system is a Hydrostatic Transmission (HST) system coupled with a pump. It consists of a hydraulic motor with a pump, and a Programmable Logic Controller (PLC)—operated panel. Figure 1 shows the HST system. The circuit diagram is shown in Fig. 2. In the system, two types of valves are used, namely directional control valve (DCV) and flow control valve (FCV). The set pressure can be varied using Pressure Relief Valve (PRV). The pressure transducer is incorporated to measure the inlet, output, and delivery side pressures (P_{mi}, P_{mo}, and P_{pp} respectively). The motor speed (*vm*) is evaluated using a speed sensor (Table 1).

2 Modeling of the System

Modeling is a crucial and troublesome step because of the complication of the monitored system when it is coupled with different control equipment. As a result, in order to create a reduced order process model that can faithfully replicate essential process dynamics under specific operating conditions, there must be some trade-off.

Utilizing effort and flow constraints, power conservation is an essential feature of bond graph models. Because of this, modeling physical processes and multidisciplinary dynamic engineering systems with sub-systems or components from various energy domains are best achieved through the Bond graph. Therefore, Bond graph modeling is employed to design the hydraulic drive system.

S. Paul (✉) · A. Mondal · A. Guha · P. K. Dubey
Department of Mechanical Engineering, Asansol Engineering College, Asansol 713305, India
e-mail: sarnendu.me@aecwb.edu.in

S. K. Ghoshal et al. (eds.), *Recent Advances in Industrial Machines and Mechanisms*,
Lecture Notes in Mechanical Engineering,
https://doi.org/10.1007/978-981-99-4270-1_14

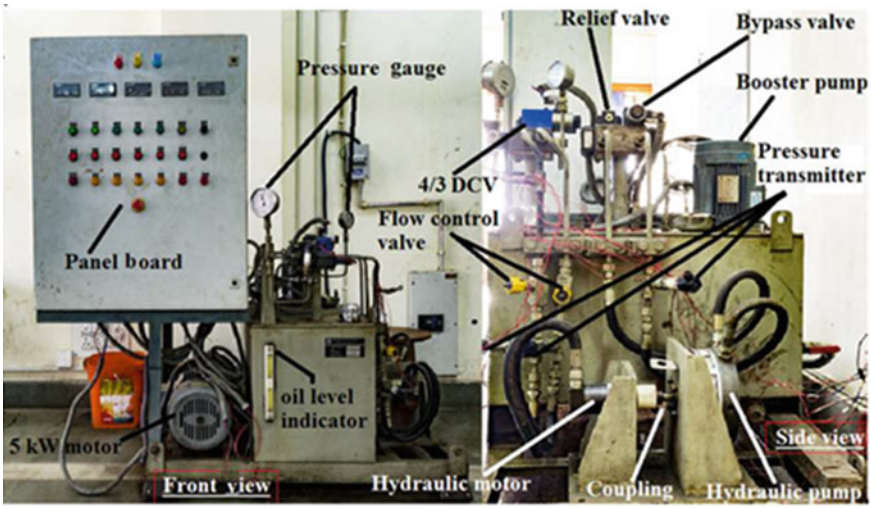

Fig. 1 The hydrostatic transmission system

3 Generation of System Equations from Bond Graph Model

In this chapter, square root type nonlinearity is considered to model all the solenoid-operated Directional Control Valves (DCVs) and Pressure Relief Valves (PRVs) as given in Eq. (1) in its general form.

$$\dot{V} = C_d A \sqrt{\frac{2|\Delta P|}{\rho}} \text{sgn}(\Delta P) = k\sqrt{\Delta P}\,\text{sgn}(\Delta P) \tag{1}$$

where V is the volume flow rate, C_d is the coefficient of discharge, A is the port area, ρ is the density of oil, ΔP is the pressure differential, sgn(ΔP) is the sign function returning positive and negative values and k is a parameter.

The Sf_2, and Sf_{15} are the sources of flow, expressed as:

$$\text{Sf}_2 = k_\text{fi}\sqrt{|P_\text{supl} - P_\text{mi}|}\,\text{sgn}\big(P_\text{supl} - P_\text{mi}\big) \tag{2}$$

$$\text{Sf}_{15} = k_\text{fo}\sqrt{|P_\text{mo} - P_\text{s}|}\,\text{sgn}(P_\text{mo} - P_\text{s}) \tag{3}$$

where k_fi and k_fo relate to the inlet and outlet of the DCV, respectively. So, it is considered that the k values are identical, $k_\text{fi} = k_\text{fo} = k_\text{f}$.

According to the bond graph model of the system in Fig. 3, the flow variable (f) is replaced by volume flow rate V. The proceedings are as follows:

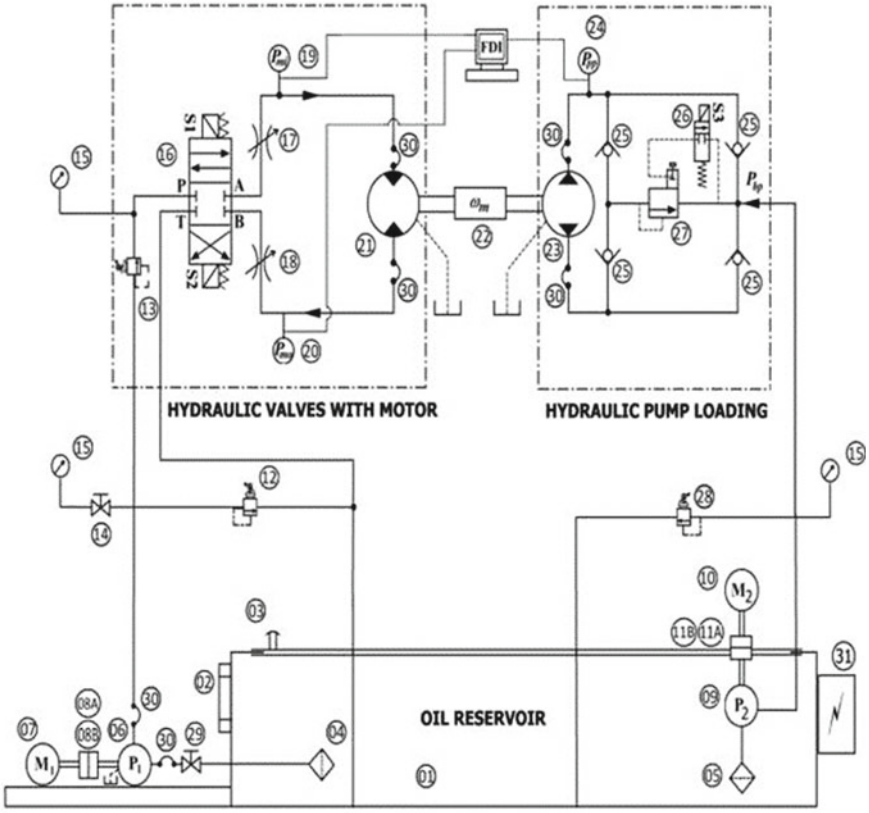

Fig. 2 The circuit diagram of the system

Table 1 Summary of system specification

Oil reservoir capacity	0.1 m^3 (100 L)
Pump flow	2.5 × 10–4 m^3/s (15 lpm)
Electrical motor capacity	5.5 kW
Maximum working pressure	2 × 106 kg/ m^2
Electrical motor rating	7.5 kW
Voltage	415 V, 3-Phase, 50 Hz
Control voltage	24 V DC
Hydraulic oil type Servo system	VG 68

(a) For the C_4 element, the system gives the flow f_4, which can be expressed as:

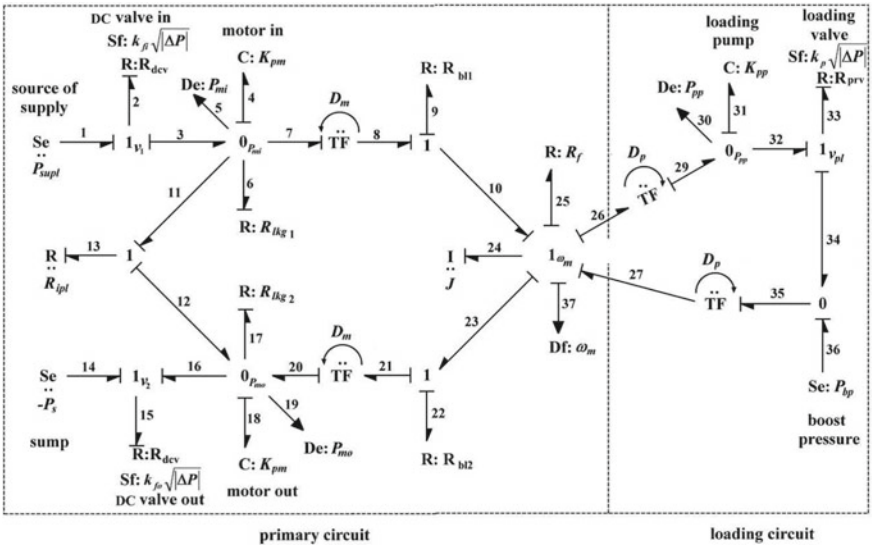

Fig. 3 The bond graph model of the system

$$\Rightarrow \frac{\dot{P}_{\mathrm{mi}}}{K_{\mathrm{pmi}}} = k_{\mathrm{fi}}\sqrt{\left|P_{\mathrm{supl}} - P_{\mathrm{mi}}\right|}\mathrm{sgn}\left(P_{\mathrm{supl}} - P_{\mathrm{mi}}\right) - D_m\omega_m - \frac{P_{\mathrm{mi}}}{R_{\mathrm{lkg1}}} - \frac{P_{\mathrm{mi}} - P_{\mathrm{mo}}}{R_{\mathrm{ipl}}} \tag{4}$$

In the Eq. (4), f_3 represents the inward flow through the DC valve (i.e., Sf_2), $f_7 = (D_{\mathrm{m}}\omega_{\mathrm{m}})$ indicates the flow output from the hydro-motor, $f_6 = (P_{\mathrm{mi}}/R_{\mathrm{lkg1}})$ the external leakage loss and $f_{11} = (P_{\mathrm{mi}} - P_{\mathrm{mo}})/R_{\mathrm{ipl}})$ the cross-port leakage through the valve ports. The terms R_{lkg1} and R_{ipl} represent the resistances in the external leakage flow path and cross-port path, respectively.

(b) For the C_{18} element the system gives the flow f_{18}, which can be expressed as:

$$\Rightarrow \frac{\dot{P}_{\mathrm{mo}}}{K_{\mathrm{pmo}}} = D_m\omega_m - K_{\mathrm{fo}}\sqrt{|P_{\mathrm{mo}} - P_s|}\mathrm{sgn}(P_{\mathrm{mo}} - P_s) - \frac{P_{\mathrm{mo}}}{R_{\mathrm{lkg2}}} + \frac{P_{\mathrm{mi}} - P_{\mathrm{mo}}}{R_{\mathrm{ipl}}} \tag{5}$$

In the above equation, f_{16} represents the outward flow through the DC valve (i.e., Sf_{15}), $f_{17} = (P_{\mathrm{mo}}/R_{\mathrm{lkg2}})$ the external leakage loss of hydro motor output. The term R_{lkg2} represents the leakage resistance along the delivery side of the hydro motor.

(c) For the C_{31} element, the system gives the flow f_{31}, which can be expressed as:

$$\Rightarrow \frac{\dot{P}_{\mathrm{pp}}}{K_{\mathrm{pp}}} = D_{\mathrm{p}}\omega_{\mathrm{m}} - k_{\mathrm{P}}\sqrt{\left|\left(P_{\mathrm{pp}} - P_{\mathrm{bp}}\right)\right|}\mathrm{sgn}\left(P_{\mathrm{pp}} - P_{\mathrm{bp}}\right) \tag{6}$$

where D_p represents the pump displacement in the loading circuit, ω_m is the speed of the hydro-motor, k_p is the flow coefficient of the loading valve (i.e., $k_p = f(C_d, A, \rho)$) and k_{pp} is the bulk stiffness of the fluid along the loading pump plenum. The term P_{pp} is the pressure at the loading pump plenum P_{bp} is the pressure supplied by the gear and pump.

(d) For the I_{24} element, the system gives the effort e_{24}, which can be expressed as:

$$J\omega_m = D_m(P_{mi} - P_{mo}) - R_f\omega_m - (R_{bl1} + R_{bl2})\omega_m - D_P\left(P_{PP} - P_{bp}\right) \quad (7)$$

Thus, Eqs. 4, 5, 6, and 7 are the system equations.

4 Analytical Redundancy Relations (ARRs)

ARRs are the fine constraint laws that are expressed in an iconic format with only the parameters and variables [8–11]. They are written symbolically as ARR: f ($\boldsymbol{U}$, $\boldsymbol{\theta}$, $\boldsymbol{Y}$), where $\boldsymbol{U} = [u_1, u_2, u_3, \ldots]\ T$ the input matrix, $\boldsymbol{\theta} = [\theta_1, \theta_2, \theta_3, \ldots]\ T$, is the parameter matrix and $\boldsymbol{Y} = [y_1, y_2, y_3, \ldots]\ T$ is the affair matrix. Due to the noises, the residual values have errors. Finally, the coherence vector $C = [c_1, c_2, c_3, \ldots]$ is generated to identify alarm conditions. Thereafter, by treating the residual noises the problem can be minimized.

A decision procedure, $C = \Phi\ (\mathrm{Rd}_1, \mathrm{Rd}_2, \ldots, \mathrm{Rd}_n)$ is used to check the sensitivity of the residuals. An adaptive threshold [10–13] denoted by $\pm\varepsilon_i\ (t, \mathrm{Se}, \mathrm{Sf}, u)$ is employed so that the residual, also known as robust residual, is sensitive to a fault yet unaware of parametric concerns.

The elements of C, c_i $(i = 1 \ldots n)$, are figured from:

$$c_i = \left[\begin{matrix} 1 \text{ if } |\mathrm{Rdi}| > |\varepsilon_i(t, Se, Sf, u)| \\ 0 \quad \text{otherwise} \end{matrix}\right] \quad (8)$$

when $C \neq [0, 0, \ldots]$, there is a fault. The Fault Signature Matrix (FSM), S which creates a structure that connects disagreement in factors to changes in leftovers, brings the process to a successful conclusion.

$$S_{ji} = \left[\begin{matrix} 1 \text{ if } i\text{th ARR contains } j\text{th component} \\ 0 \quad \text{otherwise} \end{matrix}\right] \quad (9)$$

5 The Adaptive Threshold for Robust Residual

In this paper, adaptive thresholds are designed using the Linear Fractional Transformation (LFT) model using established methodology [10–13] (Fig. 4). The bond graph model in Fig. 3 is shown in LFT form in Fig. 5.

The ARRs from the bond graph model using the unique methodology, including parametric uncertainty described in [8–11].

$$\mathrm{ARR}_1 : \left(k_{fi}\sqrt{\left|P_{\mathrm{supl}} - P_{\mathrm{mi}}\right|}\,\mathrm{sgn}\left(P_{\mathrm{supl}} - P_{\mathrm{mi}}\right) - D_{\mathrm{m}}\omega_{\mathrm{m}} - \frac{P_{\mathrm{mi}}}{R_{\mathrm{lkg}}} - \frac{P_{\mathrm{mi}} - P_{\mathrm{mo}}}{R_{\mathrm{ipl}}} - \frac{\dot{P}_{\mathrm{mi}}}{K_{\mathrm{pm}}} \right) + \alpha_1 = 0 \tag{10}$$

Fig. 4 The LFT model

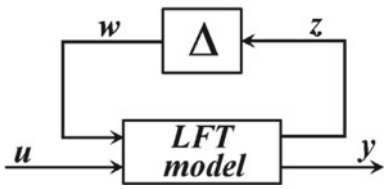

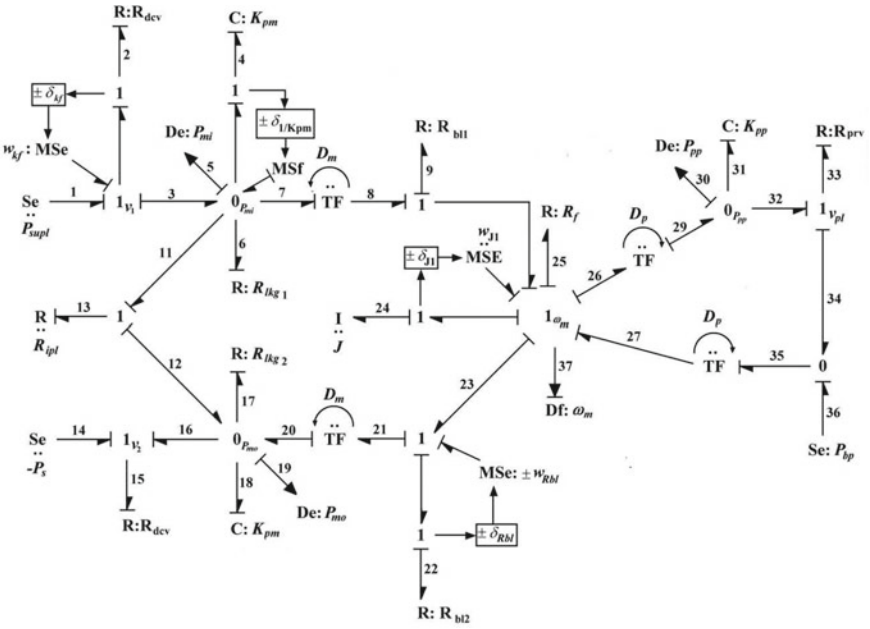

Fig. 5 LFT form of the Bond graph model

$$\mathrm{ARR}_2 : \left(D_\mathrm{m}\omega_\mathrm{m} - \frac{P_\mathrm{mo}}{R_\mathrm{lkg}} - K_\mathrm{fo}\sqrt{|P_\mathrm{mo} - P_\mathrm{s}|}\mathrm{sgn}(P_\mathrm{mo} - P_\mathrm{s}) + \frac{P_\mathrm{mi} - P_\mathrm{mo}}{R_\mathrm{ipl}} - \frac{\dot{P}_\mathrm{mo}}{K_\mathrm{pm}} \right) + \alpha_2 = 0 \tag{11}$$

$$\mathrm{ARR}_3 : \left(D_\mathrm{p}\omega_\mathrm{m} - k_\mathrm{P}\sqrt{\left|\left(P_\mathrm{pp} - P_\mathrm{bp}\right)\right|}\mathrm{sgn}\left(P_\mathrm{pp} - P_\mathrm{bp}\right) - \frac{\dot{P}_\mathrm{pp}}{K_\mathrm{pp}} \right) + \alpha_3 = 0 \tag{12}$$

$$\mathrm{ARR}_4 : (D_\mathrm{m}(P_\mathrm{mi} - P_\mathrm{mo})) - \omega_\mathrm{m}(2R_\mathrm{bl} + R_\mathrm{f}) - D_\mathrm{P}(P_\mathrm{mi} - P_\mathrm{mo}) - J\omega_\mathrm{m}) + \alpha_4 = 0 \ldots (13) \tag{13}$$

where,

$$\alpha_1 = \left| \delta_\mathrm{kf} \left(k_\mathrm{f}\sqrt{|P_\mathrm{supl} - P_\mathrm{mi}|} \right) \right| + |\delta_\mathrm{Dm}(D_\mathrm{m}\omega_\mathrm{m})| + \left|\delta_{1/\mathrm{Kpm}} P_\mathrm{mi}/K_\mathrm{pm}\right| \tag{14}$$

$$\alpha_2 = \left| \delta_\mathrm{Dm} \left(D_\mathrm{m}\, \dot{\omega}_\mathrm{m} \right) \right| + \left| \delta_{kf} \left(kf\sqrt{|P_\mathrm{mo} + P_\mathrm{s}|} \right) \right| + \left|\delta_{1/\mathrm{Kpm}} P_\mathrm{mo}/K_\mathrm{pm}\right| \tag{15}$$

$$\alpha_3 = \left|\delta_\mathrm{Dp}\left(D_p\omega_m\right)\right| + \left| \delta_\mathrm{kp} \left(k_p\sqrt{|P_\mathrm{pp} - P_\mathrm{bp}|} \right) \right| + \left|\delta_{1/\mathrm{Kpp}} P_\mathrm{pp}/K_\mathrm{pp}\right| \tag{16}$$

$$\alpha_4 = |\delta_\mathrm{Dm} D_\mathrm{m}(P_\mathrm{mi} - P_\mathrm{mo})| + |\omega_n(\delta_\mathrm{rbl}(2R_\mathrm{bl}) + \delta_\mathrm{rf}R_\mathrm{f}| + \left|\delta_\mathrm{Dp}(D_\mathrm{p}(P_\mathrm{pp} - P_\mathrm{bp}))\right| + \left|\delta_\mathrm{j}(J\, \dot{\omega}_m)\right| \tag{17}$$

The derived ARRs are divided into two parts: the nominal part (ARR_in: $i = 1..4$) and uncertain parts (α_i, $i = 1..4$).

$$Rd_\mathrm{iu} = Rd_\mathrm{in} + a_\mathrm{i},\ Rd_\mathrm{il} = Rd_\mathrm{in} - a_i.$$

If the residual value derivates more than the uncertainty limit, it will hit the threshold level and be deemed faulty. Figure 6 provides a schematic representation of the conclusion cycle.

6 Validation Through Experimentation and Model Simulation

The Fault Signature Matrix (FSM) is constructed from ARRs given in Eq. (14–17) given in Table 2. All of the postulated faults' signatures are isolable in the event of a single fault (blocking Rbl and Rf). For multi-fault versions of the coherence vector $C = [0\ 0\ 1\ 1]$, the concealed part of Table 2 consists of the faulty parameters k_p, Rbl, D_p, and Rf that cannot be isolated. The flow control valve (item No. 17 in Fig. 2) is

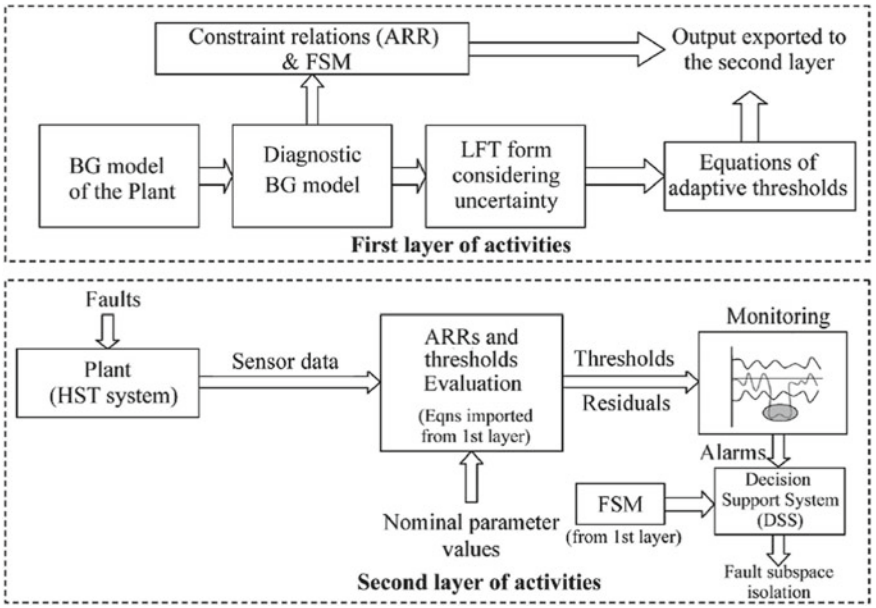

Fig. 6 Activities related to system identification

manually opened to cause a blockage fault that results in a mode shift in the hydraulic motor's supply line. The flow path was partially and gradually closed over the course of 50 s, which is what produced this defect. The loading circuit then experiences an abrupt blockage problem as a result of the change in k_p after the loading circuit bypass valve (item No. 26 in Fig. 2) is turned off after 100 s. It's crucial to keep in mind that the second fault develops without the previous one being fixed: between 50 and 100 s, one component degrades, and after 100 s, trials with multiple faults take place.

To relate the test data with the simulation model, the bond graph model (Fig. 3) is converted to a MATLAB-Simulink model shown in Fig. 7. In order to further

Table 2 Fault signature matrix of the system

	Rd_1	Rd_2	Rd_3	Rd_4	M_b	I_{bs}	I_{bm}
k_p	0	0	1	0	1	1	0
R_{bl}	0	0	0	1	1	1	0
R_f	0	0	0	1	1	1	0
D_p	0	0	1	1	1	1	0
k_f	1	1	0	0	1	1	0
D_m	1	1	0	1	1	1	0

demonstrate the noise filtration, the comparisons are made between the test data and the simulation-based replies and illustrated in Fig. 8.

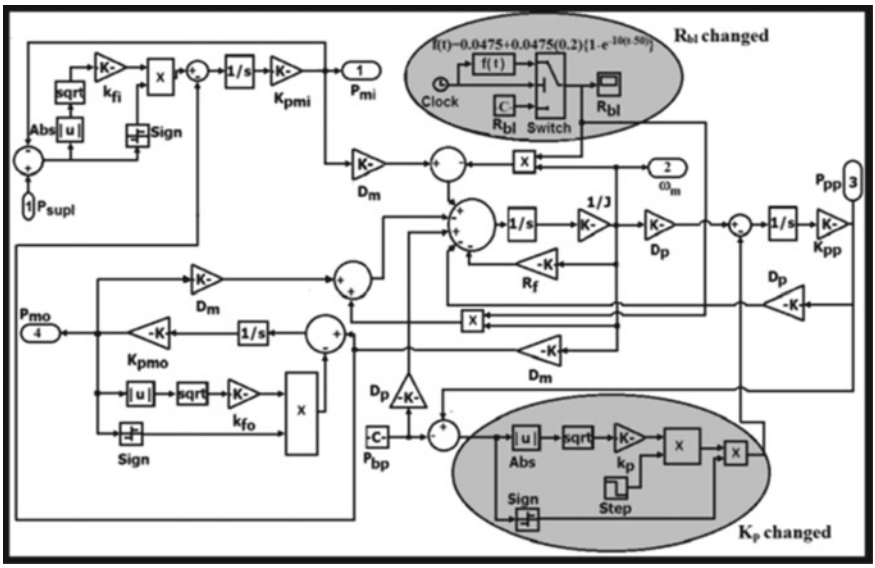

Fig. 7 MATLAB-Simulink model of the system

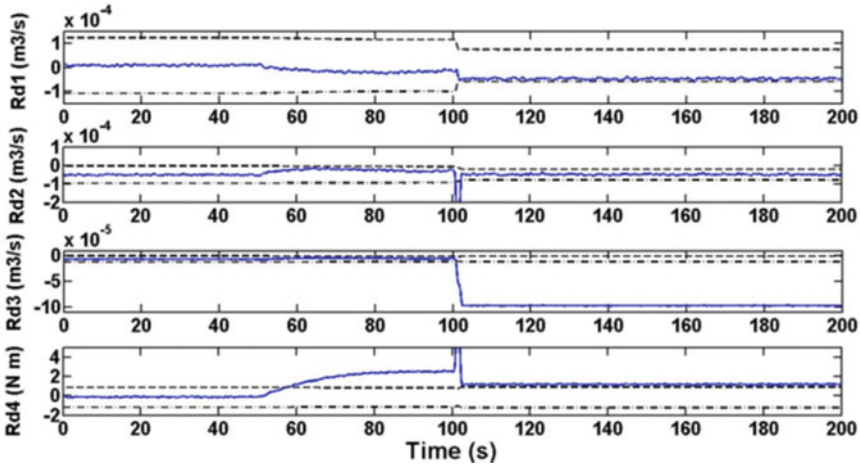

Fig. 8 Normal and faulty mode responses

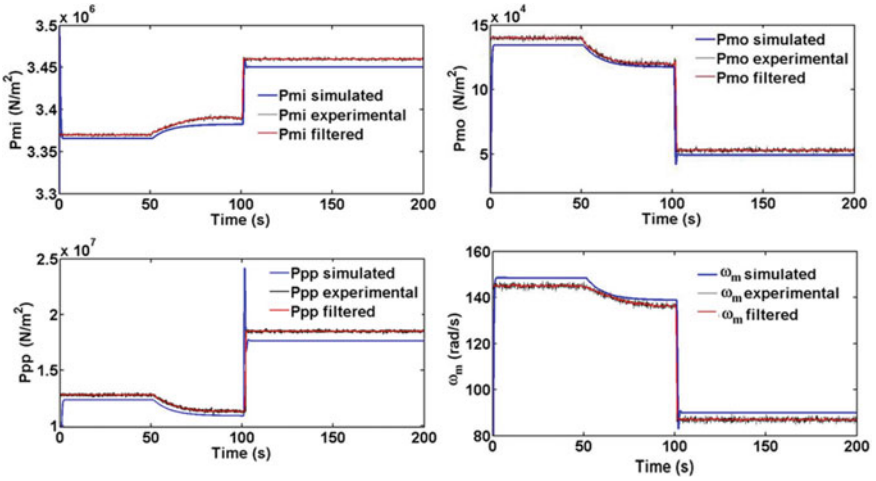

Fig. 9 Variation of residuals in normal and faulty mode

7 Conclusions

In this chapter, a bond graph model is implemented for the generation of fault indicators on a HST system. The Fault Detection and Isolation (FDI) methodology is discussed during this work. The bond graph model is redrawn in Linear Fractional Transformation (LFT). The uncertainties are not considered and the absolute values of the uncertain parts are only considered. An uncertain part and a nominal part are created simultaneously when Analytical Redundancy Relations (ARRs) are generated. A method of choosing is demonstrated, which compares each residual against a threshold to produce the coherence vector C. Detection of a fault occurs when, $C \neq [0, 0, \ldots]$. An in-depth comparison between the simulation response and the speculative dimension is established (Fig. 9).

References

1. Venkatasubramanian V, Rengaswamy R, Yin K, Kavuri SN (2003) A review of process fault detection and diagnosis: part I: quantitative model-based methods. Comput Chem Eng 27(3):293–311
2. Shi Z, Gu F, Lennox B, Ball AD (2005) The development of an adaptive threshold for model-based fault detection of a nonlinear electro-hydraulic system. Contro Eng Pract 13(11):1357–1367
3. Athanasatos P, Costopoulos T (2012) Proactive fault finding in a 4/3-way direction control valve of a high-pressure hydraulic system using the bond graph method with digital simulation. Mech Mach Theory 50:64–89
4. Ould-Bouamama B, Medjaher K, Samantaray AK, Staroswiecki M (2006) Supervision of an industrial steam generator. Part I: bond graph modeling. Control Eng Pract 14(1):71–83

5. Nawaz MH, Yu L, Liu H, Rehman WU (2017) Analytical method for fault detection & isolation in electro-hydrostatic actuator using bond graph modeling. In: Applied Sciences and technology (IBCAST), IEEE 14th international bhurban conference on applied sciences and technology, pp 312–317
6. Wang D, Yu M, Low CB, Arogeti S (2013) Model-based health monitoring of hybrid systems. Springer, New York
7. Watton J (2007) Fluid power systems. Prentice Hall, p 142
8. Ould-Bouamama B (2003) Bond graph approach as an analysis tool in thermo-fluid model library conception. J Franklin Inst 340:1–23
9. Samantaray AK, Medjaher K, Ould-Bouamama B, Staroswiecki M, Dauphin-Tanguy G (2006) Diagnostic bond graphs for online fault detection and isolation. Simul Model Pract Theory 14(3):237–262
10. Samantaray AK, Ould-Bouamama B (2008) Model-based process supervision: a bond graph approach. Springer Science & Business Media
11. Ghoshal SK, Samanta S (2011) Robust fault diagnosis and prognostics of a hoisting mechanism: a simulation study. Int J Eng Sci Technol IJEST 3(2):962–980
12. Djeziri MA, Merzouki R, Ould-Bouamama B, Dauphin-Tanguy G (2006) Fault detection of backlash phenomenon in a mechatronic system with parameter uncertainties using bond graph approach. In: Mechatronics and automation, proceedings of the 2006 IEEE international conference, pp 600–605
13. Djeziri MA, Ould-Bouamama B, Dauphin-Tanguy G, Merzouki R (2011) LFT bond graph model-based robust fault detection and isolation. Bond graph modelling of engineering systems. Springer, New York, pp 105–133